Journal of Translational Medicine

RESEARCH

Open Access

Apelin-13 attenuates optic nerve damage in glaucomatous mice by regulating glucose metabolism

Ya Zhang[1,2], Jia Zhao[3], Jian Zhou[4], Zhen Jiang[2], Kaihui Cheng[2], Caifeng Lei[1] and Ling Yu[1*]

Abstract

Background In patients with advanced glaucoma, lesions frequently extend beyond the eye and affect other organs. However, early distal consequences of elevated intraocular pressure (IOP) remain unclear. This study aimed to observe glucose uptake in the optic cortex during the early stages of elevated IOP and to investigate the mechanism by which Apelin13 exerts neuroprotective effects.

Methods This study used a single anterior chamber injection of polystyrene microbeads and triblock copolymer hydrogel in 6- to 8-week-old male C57BL/6J mice and observed glucose uptake in the optic cortex during the initial phase of IOP elevation using micro-positron emission tomography/magnetic resonance imaging (PET/MRI). Pathological changes in the optic nerve and optic cortex were assessed by immunofluorescence, reactive oxygen species (ROS) kit, and and nicotinamide adenine dinucleotide phosphate (NADPH) kit. Expression of glucose transporter proteins (GLUTs) and key enzymes of the pentose phosphate pathway (PPP) was evaluated using immunofluorescence and western blot. The activation of the phosphatidylinositol 3-kinase (PI3K)/protein kinase B signaling pathway was analyzed via western blot.

Results On day 1 of elevated IOP, the modeled eye exhibited reduced glucose uptake in the corresponding visual cortex compared with the contralateral visual cortex. Over time, the condition gradually improved, with no discernible difference between the two sides by day 21. Concurrently, along with abnormal activation of microglia and progressive reduction of retinal ganglion cells, we noted abnormal expression of glucose transporter proteins in visual cortical neurons. Additionally, elevated levels of ROS and NADPH were observed in both the retinal and brain tissues following IOP elevation. In contrast, administration of the neuroprotectant Apelin-13 mitigated the pathology induced by IOP elevation. Conversely, treatment with a PI3K inhibitor significantly diminished the protective effects of Apelin-13.

Conclusions These findings imply that altered glucose metabolism in the visual center may be an early sign of optic nerve damage in patients with glaucoma. Apelin-13 may rely on the PI3K/Akt signaling pathway to regulate the redistribution of energy metabolism in the retina and visual centers, thereby mitigating oxidative stress and safeguarding neuronal cells.

*Correspondence:
Ling Yu
oculistlingyu@Hotmail.com

Full list of author information is available at the end of the article

Keywords Apelin-13, Energy metabolism, Retinal ganglion cells, Glucose transporter, GLUT1, GLUT3

Introduction

Glaucoma is a chronic, sight-threatening condition that results from the progressive loss of retinal ganglion cells (RGCs) and often leads to irreversible visual impairment. It is the third most common cause of visual deficits worldwide, after cataracts and uncorrected refractive errors [1]. Elevated intraocular pressure (IOP) remains the sole modifiable risk factor for glaucoma. Despite medical and surgical interventions aimed at reducing IOP, disease progression persists, and no clinically approved treatment directly enhances RGCs survival [2]. Recent studies have explored various strategies beyond IOP reduction to prevent RGCs loss, demonstrating the efficacy of various neuroprotective agents and their mechanisms in cellular and animal models [3].

Primary neuronal injury exerts profound effects on distal neurons interconnected via synapses, a phenomenon termed transsynaptic or transneuronal degeneration. This process has been implicated in the propagation of pathologies across various neurological conditions, including glaucoma [4]. Recent studies have highlighted that glaucoma manifests not only as an ocular pathology but also as damage to brain structures. The absence of optic nerve fibers comprising RGCs axons leads to the degeneration of neurons projecting to central visual targets throughout the optic nerve [5]. Thus, early interventions, prior to substantial RGCs loss, present a critical strategy for preventing damage from spreading across synapses to target neurons. Strategies combining IOP reduction with treatments that safeguard retinal and central visual system neurons offer promising avenues to prevent glaucomatous blindness [6].

The brain, including the retina, is among the body's most energy-demanding tissues, consuming up to 20% of its total oxygen supply [7]. Energy expenditure in the retina is similar to that in the brain, even with greater energy requirements than those of brain tissues. When oxygen supply and metabolite levels fail to meet the high energy demands of retinal neurons, retinal neuron function is often severely compromised [8]. RGCs are specialized projection neurons crucial for transmitting visual information to the brain. Approximately 90% of all sensory signals integrated into the brain are derived from vision, and almost one-third of the cerebral cortical surface is used for visual processing [9]. RGCs and the brain constitute a strongly interconnected network. Glaucoma not only affects the retina but also causes abnormalities in the brain [6]. Metabolic changes or functional abnormalities have been observed in the brains of patients with glaucoma [10]. Therefore, pathological changes in the brain should be a focus of future glaucoma research.

Although the precise pathogenesis of glaucoma remains unclear, evidence underscores impaired bioenergetics at the RGCs level as a significant contributing factor. Recent findings suggested compromised blood flow to the choroid, retina, and optic nerve in some patients with glaucoma [11]. This compromised blood flow could induce tissue ischemia and hypoxia, exacerbating energy metabolism damage due to insufficient blood supply. Similarly, endogenous bioenergetic deficits also play a prominent role. Paracrine axonal transport is the process by which motor proteins (kinesins) in microtubules deliver transport proteins, mitochondria, and other vital substances to the distal synapses. The absence of energy is an important reason for the failure of axonal transport [12]. Mitochondrial and metabolic deficiencies are common in glaucoma pathogenesis, with strategies aimed at rectifying these deficits showing promise in cellular and animal models of glaucoma, supporting the notion that bioenergetic deficits predispose RGCs to glaucomatous neurodegeneration [13].

In addition, in mice with elevated IOP, dysfunctional mitochondria trigger hypoxia-glucose deprivation in the retina, including the production and accumulation of non-physiological reactive oxygen species (ROS). Excessive ROS generation induces oxidative stress, which contributes to RGCs loss [14]. Our previous studies corroborated these findings [15]. Oxidative stress, characterized by an imbalance between ROS production and elimination, necessitates additional reducing capacity, with the pentose phosphate pathway (PPP) emerging as a major contributor. Increased glucose flow through the PPP may exert neuroprotective effects under oxidative stress conditions [16, 17]. Understanding energy metabolism in the visual conduction pathway, notably in neurons and RGCs, is pivotal for understanding the pathophysiological process of glaucoma, with targeting metabolic dysfunctions representing a viable strategy to prevent axonal degeneration and preserve visual function.

Apelin is a biologically active neuropeptide that acts as an endogenous ligand for APJ [18]. Among its isoforms, Apelin-13 exhibits the highest concentration and plays a pivotal role in neuroprotection [19]. Apelin deficiency correlates with reduced motor neuron numbers and earlier disease onset, while Apelin-13 administration significantly protects the blood-brain barrier (BBB) integrity by decreasing its permeability from damage and delays disease progression [20]. Additionally, Apelin-13 acts as an anti-inflammatory and neuroprotective agent that regulates glycolipid metabolism. Both endogenous and exogenous Apelin-13 are protective against N-methyl-D-aspartate (NMDA)-induced RGCs loss, which may be

mediated through the regulation of TNF-α expression [21, 22].

Overall, existing evidence demonstrates the protective effects of Apelin-13 against glaucomatous optic nerve injury, although the underlying mechanisms remain elusive. In this study, we utilized a mouse glaucoma model, as described in our previous study [23], to simulate the onset of clinical glaucoma and explore whether Apelin-13 exerts neuroprotective effects by regulating the redistribution of energy metabolism in nerve cells.

Methods

Experimental animals

All animal studies were conducted in compliance with the guidelines outlined in the Statement on the Use of Animals by the Association for Research in Vision and Ophthalmology (ARVO) and were approved by the Animal Use and Care Committee of Southwest Medical University. We used 6–8-week-old male C57BL/6J mice obtained from Chongqing Tengxin Biological Company. The mice were bred and housed in a controlled environment with a 12-hour light/dark cycle and maintained at regulated temperature and humidity.

Anterior chamber injection in mice

The specific protocol for establishing the mouse glaucoma model is detailed in our previous study [23]. Briefly, Randomly selected 6–8 weeks C57BL/6J male mice as the experimental or control group. Mice were anesthetized intraperitoneally and received ocular surface anesthesia. A sterile 34G needle (World Precision Instruments; USA) was attached to a 10-μL microsyringe, and polystyrene microbeads (1.0×10^4, 1 μL/eye) and triblock copolymer hydrogel **PEG-PCL-PEG** (PECE) (1 μL/eye) were injected into the anterior chamber of the randomly selected left or right eyes, with the control eye receiving a saline injection.

Mouse vitreous injection

After general and ocular surface anesthesia were administered to the mice, 1 μL of fluid was injected into the vitreous cavity. Reagents for vitreous injection were taken from a study by Ishimaru et al. [21] and included [Pyr^1]-apelin-13 (10 μg/eye, MedChemExpress; Shanghai, China) dissolved in sterile saline and LY294002 (5 nmol/eye, MedChemExpress; Shanghai, China) dissolved in sterile dimethyl sulfoxide (DMSO). The eyes injected with sterile DMSO were used as controls. Anterior chamber injection of PECE was performed following the injection of the drug or vehicle into the vitreous cavity.

IOP measurement

Intraocular pressure (IOP) was assessed using the TonoLab rebound tonometer (Icare, Vantaa, Finland) following the protocol detailed in our previous study [24]. Briefly, IOP was recorded in mice 1 day pre-surgery and at 1, 3, and 5 days post-injection, with weekly measurements thereafter for 4 weeks. All measurements were conducted by the same researcher. To minimize bias related to circadian rhythms, the measurements were taken strictly between 9 am and 11 am. Mean values were derived from six consecutive measurements.

Retinal flat-mount preparation

The eyes were collected after the mice were executed, immersed in 4% paraformaldehyde solution, and fixed for 2 h. Subsequently, the retina was peeled off, and four symmetrical incisions were made and flattened onto slides. Retinal plates were fixed with chilled methanol, rinsed with phosphate buffered saline (PBS), sealed with a sealing solution for 2 h, and then incubated overnight at 4 °C with primary antibodies (1:200, anti-BRN3A antibody, Abcam, ab245230, UK). The following day, the primary antibody solution was removed, and the samples were washed with PBS, followed by incubation with secondary antibodies (1:500, goat anti-rabbit IgG(H + L) Dylight 488, Bioworld, China) for 2 h at room temperature under light protection. After removing the secondary antibody, the samples were washed with PBS, and the nerve fiber layer was flattened and sealed with a coverslip using a fluorescence-quenching blocking agent.

Confocal microscopy was employed for whole-retina scanning, with images acquired after superimposing the maximum projected brightness of each layer on the Z-axis and counted and analyzed using ImageJ software. A square area with a side length of 250 μm was selected in the proximal, middle, and distal sections of each quadrant of each retinal tile. Twelve areas in each retina were chosen for counting, and RGCs density per square millimeter was calculated.

Preparation of the retinal frozen section

After the mice were executed, the eyeballs were immersed in 4% paraformaldehyde for 2 h on ice. Following the removal of the anterior segment and vitreous body, eyeball cups were replaced with 30% sucrose solution for 2 h of dehydration on ice. Eye cups were embedded in OCT-tissue freezing medium and frozen at -80℃ for 2 h, then sliced into 8-μm-thick sections with a frozen slicer and mounted on slides.

Sections were warmed to room temperature for 10–30 min, rinsed with PBS, and subjected to the frozen section antigen repair solution (Beyotime, China) for 5 min, followed by washing and blocking for 2 h. Subsequently, primary antibodies (1:200, anti-BRN3A antibody, Abcam, ab245230, UK; anti-Iba1 antibody, Wako, 019-19741, Japan) were added overnight at 4 °C, followed by a 1 h incubation with secondary antibodies

(1:500, goat anti-mouse IgG(H + L) Dylight 594, goat anti-rabbit IgG(H + L) Dylight 488, Bioworld, China) at room temperature. Samples were then sealed with an anti-fluorescence-quenching sealer containing DAPI (Solarbio, China) and observed under a confocal microscope.

Frozen section of brain tissue

After the mice were executed, brain tissues were collected and fixed in 4% paraformaldehyde at 4 °C overnight, followed by gradient dehydration in 15% and 30% sucrose solutions. Following this, embedding in OCT and sectioning into 10-μm-thick slices using a frozen sectioning machine were performed.

The immunofluorescence staining procedure was performed as previously described in the "Preparation of the retinal frozen section". The primary antibodies used were Iba1(1:200, anti-Iba1 antibody, Wako, 019-19741, Japan), NeuN (1:200, anti-NeuN antibody, Cell Signaling Technology, 94403 S, USA), GLUT1 (1:100, Novus, NB110-39113, USA), GLUT3 (1:100, Novus, NBP3-12885, USA), and glucose-6-phosphate dehydrogenase (G6PD) (1:100, GeneTex, GTX101218, USA), followed by secondary antibodies (1:500, Bioworld, China).

Small animal positron emission tomography (micro-PET/CT)

The left or right eye of each mouse was randomly selected as the operative anterior chamber for injection, with the contralateral eye receiving an equivalent volume of saline as control. Differences in glucose uptake in the visual cortex of the bilateral brain were assessed via micro-PET/CT on postoperative days 1, 3, 5, 7, 14, 21, and 28. Following a 12-h fast, the mice received tail vein injections of 100–200 μCi of ^{18}F-FDG, and micro-PET/CT imaging was conducted 40 min to 1 h post-injection. PET (10 min) and CT (10 min) were performed sequentially. After final acquisition of PET images, a small animal magnetic resonance imaging (MRI) instrument was used to acquire T2-weighted imaging (T2WI) MRI images of the mouse brain.PET and MRI images were merged using the Inveon Research Workplace software (IRW), and the visual cortex on both sides of the mouse brain was localized on mouse MR images (Paxinos and Franklin, 2001). The regions of interest (ROIs) were symmetrically selected from the visual cortex on both sides of the mouse brain. The maximum SUV value (SUVmax) of each ROI was measured and normalized to the SUVmax of the cerebellum.

Western blotting

Retinal tissue and the occipital cortex contralateral to the PECE eye were collected after the mice were executed, and proteins were extracted from them. The protein concentration was adjusted to 5 μg/μL after measuring using the BCA method, and then the proteins were denatured. After gel (Vazyme, China) preparation, 20 μg of protein was added to each well of the gel for electrophoresis. Following this, the proteins were transferred to a PVDF membrane, blocked with skim milk for 1 h, washed and incubated overnight at 4 °C with primary antibodies (1:2000). The following day, the primary antibody was washed off, and the membrane was incubated with the secondary antibody (1:5000) at room temperature for 1 h, washed, and subjected to protein imaging.

NADPH content assay

The NADPH content was quantified using an NADP+/NADPH Assay Kit (WST-8 method) (Beyotime, China). Fresh retinal and brain tissues were homogenized and centrifuged, and the supernatants were assessed for NADPH content according to the manufacturer's instructions.

ROS concentration measurement

The fluorescent probe H2DCFDA targeting ROS (MedChemExpress, China) was diluted to produce a 10-μM working solution. Fresh mouse retinal and brain tissues were digested using trypsin into single-cell suspensions. One milliliter of the working solution was added to each well, incubated at 37 °C for 30 min, and centrifuged at 400 × g for 3–4 min at 4 °C. The supernatant was then removed, and the cells were washed with PBS to remove H2DCFDA that had not entered the cells and suspended by adding 1 mL of PBS. The fluorescence intensity at Ex/Em = 488/525 nm was measured using a microplate reader.

Statistical analysis

Experimental data were analyzed using SPSS 17.0 and GraphPad Prism 8.0.2 and are presented as mean ± standard deviation (SD). One-way analysis of variance was used for the overall comparison of data across multiple groups, and Tukey's multiple comparison post hoc test was used to compare data between groups. Statistical significance was set at $P < 0.05$. Data analysis was performed by personnel not involved in the experiment to ensure the accuracy and blindness of the results.

Results

Single anterior chamber injection of PECE and microbeads helped establish a stable mouse model with chronic high IOP and triggered altered glucose metabolism in the visual cortex

Baseline IOP measurements showed no significant differences between the PECE and control groups. However, post-injection, IOP in the control group fluctuated around the baseline value, whereas in the PECE group, IOP increased significantly 1 day after injection, gradually

increased peaked at 14 days, and then decreased steadily but remained high for 28 days ($P < 0.001$; Fig. 1A). Immunofluorescence staining of flat and frozen retinal sections demonstrated notable reduction in RGCs 3 days after injection in the PECE group compared with the control group ($P < 0.001$), with a trend towards further reduction over 28 days (Fig. 1B, C). In addition, microglial activation was observed 3 days after injection and became

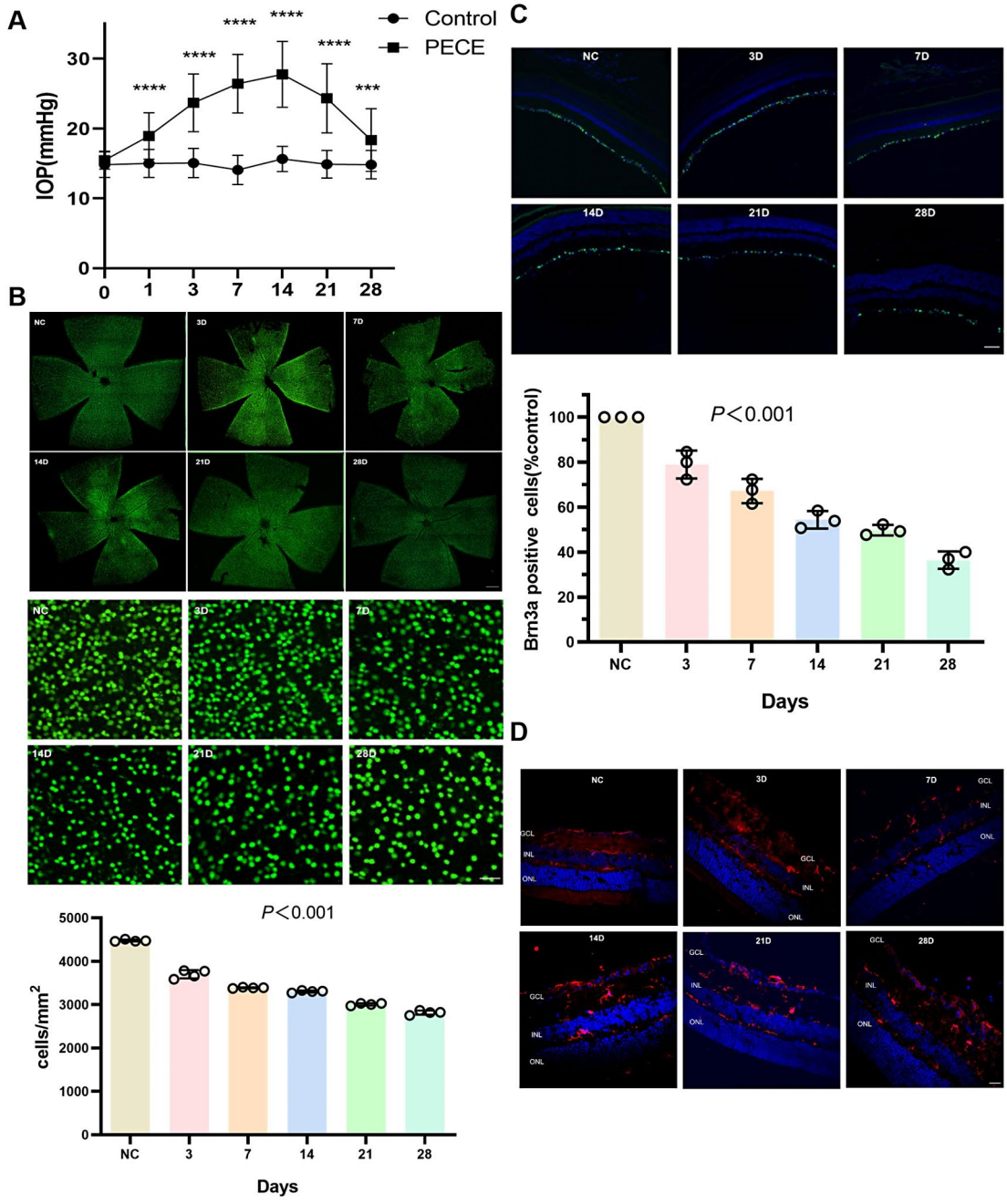

Fig. 1 IOP and pathological changes in mice after a single anterior chamber injection of PECE. (**A**): IOP remained elevated for 28 days after anterior chamber injection. $n = 28$. (**B**): Compared with the control group, a significant reduction in RGCs (green) was observed 3 days after injection in the PECE group, which worsened over 28 days. $n = 4$. Green: Brn3a; scale bar: 500 μm (up), 50 μm (down).(**C**): The number of RGCs (green) significantly decreased at 3 days post-injection in the PECE group compared with the control group, with further reductions over time. $n = 4$. Green: Brn3a; blue: DAPI; scale bar: 50 μm. (**D**): Activated microglia in the form of "amoebas" were observed in the injected eye 3 days post-injection, with branches that changed from elongated to short and stubby, and increasing in abundance at 7,14,21, and 28 days post-injection. Activated microglia (red) migrated toward the damaged ganglion cell layer. Red: Iba1; blue: DAPI; scale bar: 20 μm. ***$P < 0.001$, ****$P < 0.0001$. Error bars represent mean ± SD. DAPI: 4′,6-diamidino-2-phenylindole; GCL: ganglion cell layer; INL: inner nuclear layer; IOP: intraocular pressure; ONL: outer nuclear layer; PECE: PEG-PCL-PEG; RGCs: retinal ganglion cells; SD: standard deviation; IOP: intraocular pressure

more pronounced over 28 days, after which the microglia gradually migrated towards the damaged nodal cell layer (Fig. 1D).

Considering the physiology of optic cross-development in rodents (approximately 95% of optic nerve fibers cross to the contralateral side, compared with approximately 52% in humans and primates) [25], the diseased eyes of mice mostly affect the structure and function of the visual cortex of the contralateral hemisphere. We designated the visual cortex on the contralateral side of the operated eye as the high-IOP group and that on the ipsilateral side as the control group. No significant microglial activation was observed in the contralateral visual cortex of the affected eye within 28 days of IOP elevation (Fig. 2A). PET/MRI revealed lower glucose uptake in the visual cortex of the high-IOP group than in the control group at 1, 3, 5, 7, and 14 days post-injection. This difference was not significant at 21 or 28 days ($P < 0.05$; Fig. 2B).

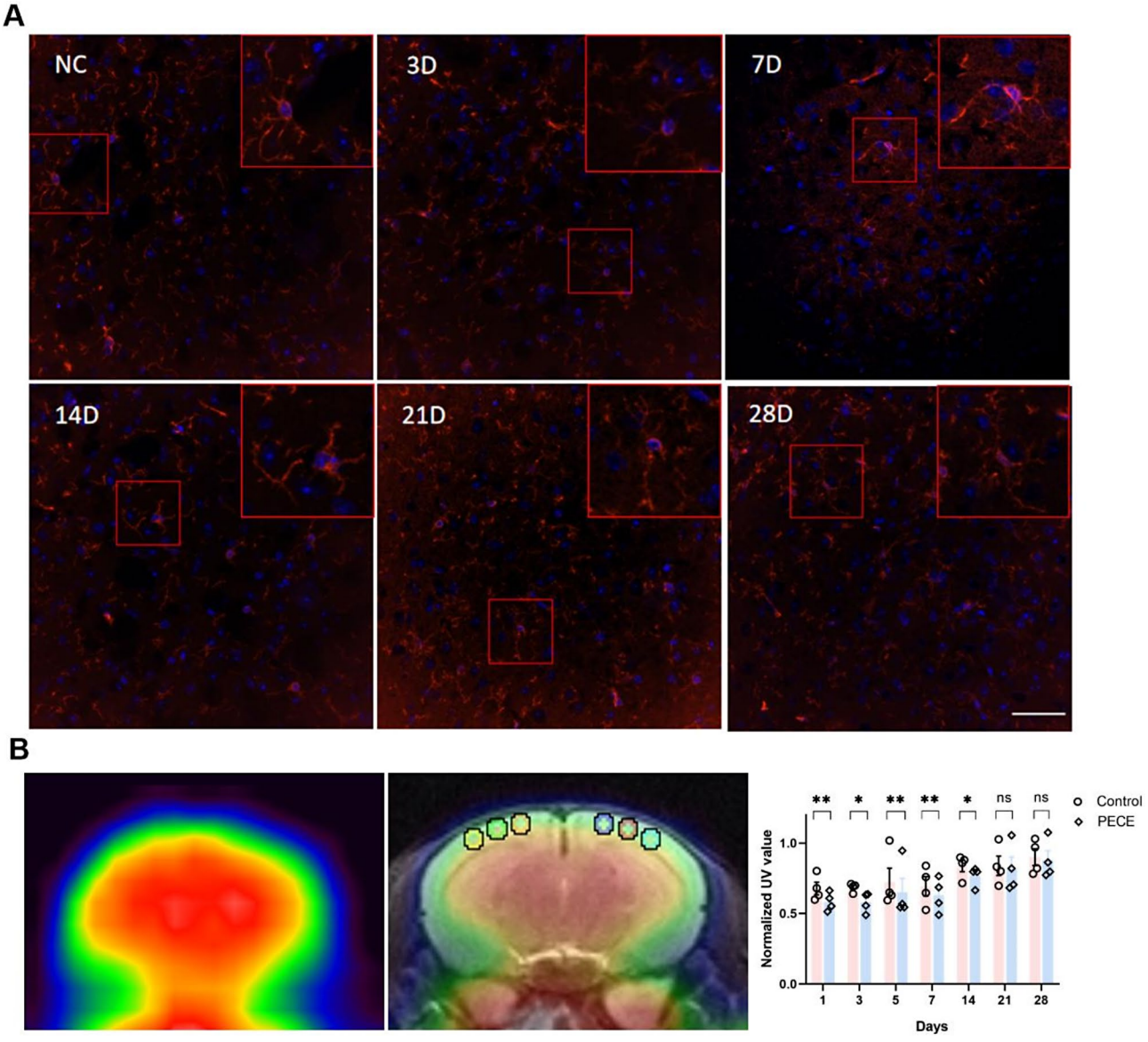

Fig. 2 Alterations in the corresponding visual cortex following elevated intraocular pressure in mice: (**A**): No significant "amoebas" microglia was observed in the contralateral visual cortex of the affected eyes within 28 days of IOP elevation compared with controls. Red: Iba1; blue: DAPI; scale bar: 50 μm. (**B**): Typical PET images and PET/MRI fusion maps of mice with elevated IOP. ROIs were selected symmetrically from both sides of the visual cortex. On postoperative days 1, 3, 5, 7, and 14, there was a difference in SUVmax between the two sides of the visual cortex, which disappeared at 21 and 28 days. $n = 4$. $^{*}P < 0.05$, $^{**}P < 0.01$. DAPI: 4′,6-diamidino-2-phenylindole; MRI: magnetic resonance imaging; PET: positron emission tomography; ROI: region of interest; SUVmax: maximum standardized uptake value

Exogenous administration of Apelin-13 reduced RGCs loss and retinal inflammatory responses induced by elevated IOP

To investigate the long-term effects of Apelin-13 on the protective effects against optic nerve injury, we observed the normal control (NC), 4-week PECE, and 4-week PECE + Apelin-13 groups. We observed a significant reduction in RGCs in the PECE group compared with the control group at 4 weeks post-injection ($P < 0.01$; Fig. 3A, B). Pre-injection administration of Apelin-13 significantly reduced RGCs loss ($P < 0.05$; Fig. 3A, B) and suppressed the activation and migration of retinal microglia (Fig. 3C) mitigating the abnormal immune response triggered by elevated IOP. In the NC group, resting microglia were observed, whereas in the PECE group, activated microglia were observed. After Apelin-13 administration, the number of activated microglia significantly reduced in the Apelin-13 group compared with the PECE group (Fig. 3C).

Exogenous administration of Apelin-13 may reverse abnormalities in glucose metabolism in visual cortex neurons and retina in response to elevated IOP

Frozen sections of brain tissues were co-stained with NeuN to observe the effect of Apelin-13 on the glucose transporter proteins GLUT1 and GLUT3 and the key enzyme of the PPP, G6PD, in visual cortical neurons. GLUT1 (Fig. 4A) and GLUT3 (Fig. 4B) expression was elevated, and G6PD (Fig. 4C) expression was decreased in the visual cortical neurons of the PECE group compared with the NC group, whereas in the Apelin-13 group, GLUT1 and GLUT3 expression was reduced, and G6PD expression was elevated. Western blotting also revealed these alterations in retinal (Fig. 4D) and brain (Fig. 4E) tissues. Compared with the control group, GLUT3 expression was elevated in both the retinal and brain tissues in the PECE group and was higher than that in the Apelin-13 group. Conversely, GLUT1 and G6PD expression was higher in the Apelin-13 group.

Apelin-13 regulated oxidative stress in retinal and brain tissues and its function may be related to the activation of the PI3K/Akt signaling pathway

Apelin-13 could regulate neuronal energy metabolism and alleviate oxidative stress induced by elevated IOP. NADPH and ROS levels were significantly elevated in the retina of mice with elevated IOP induced by PECE injection in the anterior chamber. In contrast, Apelin-13 effectively attenuated this increase in both the retinal and brain tissues (Fig. 5A and B). Additionally, activation of the PI3K/Akt signaling pathway was affected by Apelin-13 (Fig. 5C and D), whereas inhibition of the PI3K/Akt pathway by LY294002 significantly attenuated Apelin-13's ability to inhibit oxidative stress and reduce abnormalities in NADPH (Fig. 6A) and ROS (Fig. 6B) levels and reversed the regulatory effects of Apelin-13 on GLUT1, GLUT3, and G6PD (Fig. 6E and F). The protective effect of Apelin-13 on the optic nerve was significantly attenuated after inhibition of the PI3K/Akt pathway, leading to RGCs loss (Fig. 7A and B) and abnormal activation of microglia (Fig. 7C). These data suggest that Apelin-13 exerts its effects by activating the PI3K/Akt signaling pathway.

Discussion

We observed that IOP elevation for 1 day reduced glucose metabolism in the contralateral visual cortex of mice (Fig. 2B), suggesting that abnormal energy metabolism occurs in the visual conduction pathway shortly after IOP elevation. Ouyang et al. found a similar pattern, in which unilateral hypoxia reduced ^{18}F-FDG uptake ipsilaterally in mouse brain tissues during the onset of hypoxic-ischemic stroke on PET/MRI imaging [26]. We propose that reduced glucose uptake in the contralateral visual cortex of hypertensive eyes may be due to hypoxia in RGCs resulting from elevated IOP. Additionally, we observed statistically significant differences in glucose uptake on both sides until day 14, after which no significant differences were noted on days 21 and 28 (Fig. 2B), suggesting that glucose uptake in the corresponding visual cortex initially decreased and then gradually increased after IOP elevation. Notably, studies on retinal metabolomics after optic nerve crush in rodents have shown a similar trend in retinal glucose levels, indicating a reduction in the early stages, followed by an increase in the late stages of RGCs injury [27]. While previous reports have indicated reduced glucose uptake in the visual cortex of patients with advanced primary open-angle glaucoma [28], our mouse experiments showed reduced glucose uptake in the early stages of IOP elevation, followed by a tendency to level off gradually, which may be due to differences in species and glaucoma types. Furthermore, our study only observed glucose uptake in the visual cortex after 28 days. Further investigations are required to determine whether glucose uptake in the visual cortex decreases with disease progression. Nonetheless, the results of this study will help to explore the pathological mechanism of RGCs injury and find a new target for glaucoma treatment, which is early glaucoma patients may suffer from an energy deficit as well. If so, could early energy supplementation or neuroprotective agents delay the progression of glaucoma?

The retina is an extension of the nervous system that primarily relies on glucose for energy metabolism [29]. Elevated IOP can lead to ischemia and hypoxia in RGCs, resulting in inadequate energy supply and subsequent apoptosis. Recent studies have suggested that IOP-related metabolic defects play a crucial role in the susceptibility

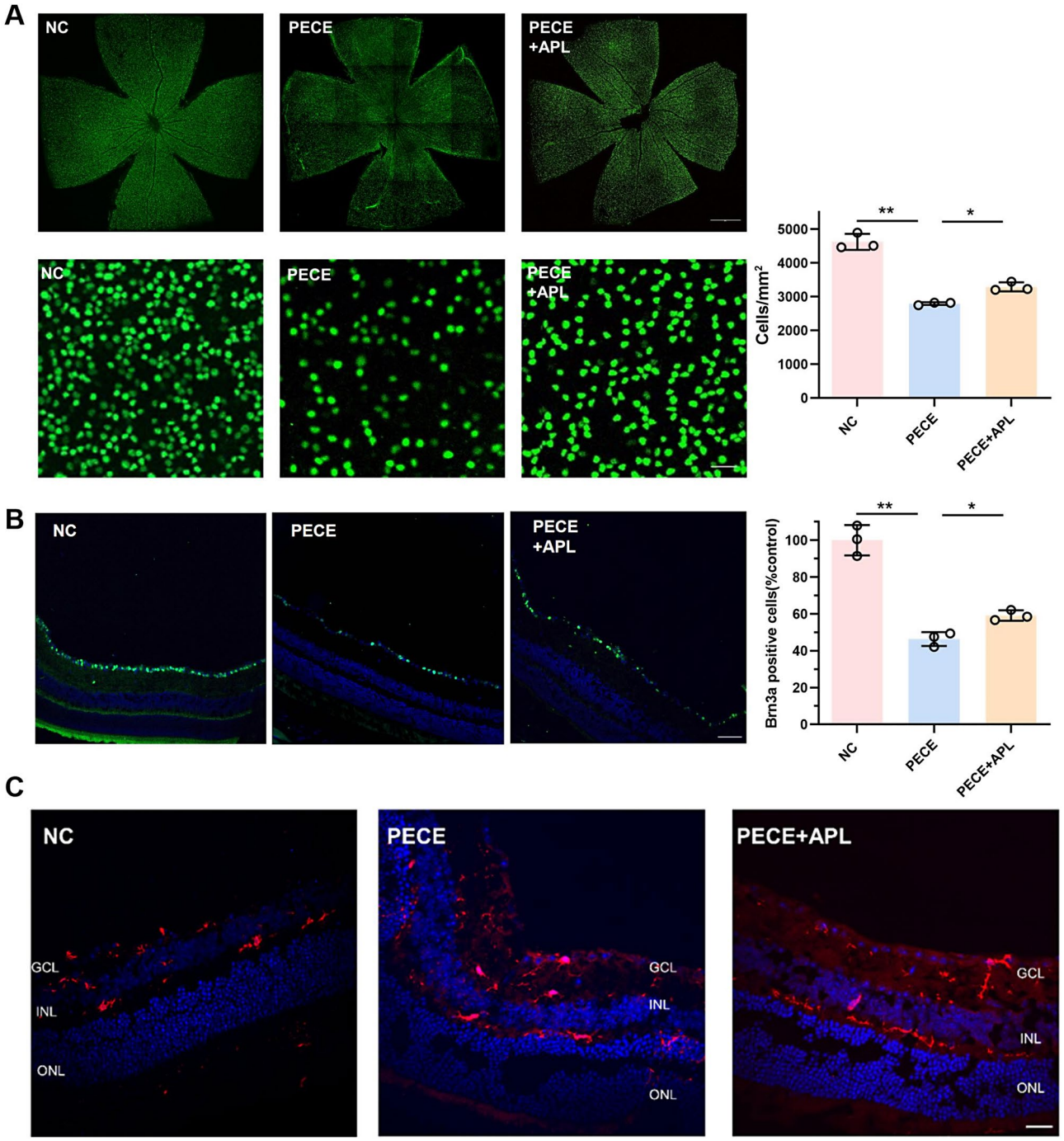

Fig. 3 Role of exogenous [Pyr1]-apelin-13 in optic nerve injury and retinal immunoinflammatory responses. (**A**) The number of RGCs was significantly lesser in the PECE group than in the control group. Moreover, the number of surviving RGCs was significantly greater in the Apelin-13 group than in the PECE group. $n=4$. (Green: Brn3a, scale bar: 500 μm in the upper panel and 50 μm in the lower panel). (**B**) The number of RGCs changed in the same manner as shown in (**A**). $n=4$. Green: Brn3a, scale bar: 50 μm. (**C**) Microglia activation was significantly inhibited in the Apelin-13 group compared with the PECE group. Red: Iba1, blue: DAPI, scale bar: 20 μm. $^{*}P<0.05$, $^{***}P<0.001$. DAPI: 4′,6-diamidino-2-phenylindole; IOP: intraocular pressure; PECE: PEG-PCL-PEG; RGCs: retinal ganglion cells

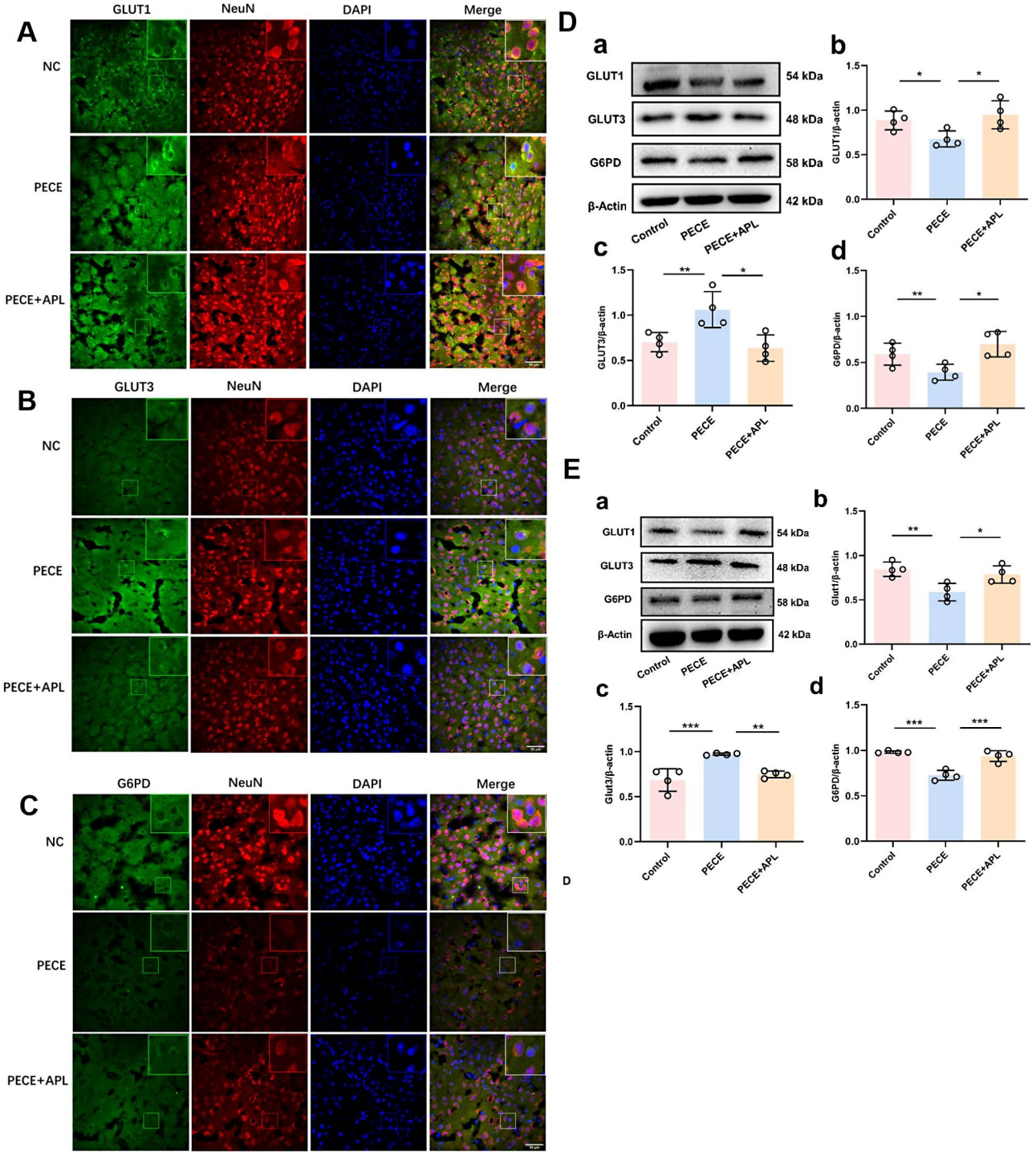

Fig. 4 Role of exogenous [Pyr1]-apelin-13 in glucose metabolism in retinal and brain neuronal cells. (**A**) GLUT1 expression in visual cortex neurons was elevated in the PECE group compared with the NC group, whereas it was lower in the Apelin-13 group than that in the PECE group. (**B**) The trend of GLUT3 expression in visual cortex neurons was consistent with that of GLUT1 expression. (**C**) G6PD expression in visual cortex neurons was lower in the PECE group than in the NC group, whereas G6PD expression was elevated in the Apelin-13 group compared with that in the PECE group. **D** a GLUT1, GLUT3, and G6PD expression in the retina. (**D**) b GLUT1 expression was decreased in the PECE group compared with the NC group and increased in the Apelin-13 group compared with that in the PECE group. (**D**) c GLUT3 expression was elevated in the PECE group compared with that in the NC group and decreased in the Apelin-13 group compared with the PECE group. (**D**) d G6PD expression was lower in the PECE group than in the NC group and increased in the Apelin-13 group compared with the PECE group. (**E** a GLUT1, GLUT3, and G6PD expression in the brain. (**E**) b c d Trend of GLUT1, GLUT3, and G6PD expression in the brain is consistent with that in the retinal tissues. *$P < 0.05$, **$P < 0.01$, ***$P < 0.001$. GLUT: glucose transporter; G6PD: glucose-6-phosphate dehydrogenase; IOP: intraocular pressure; NC: normal control; PECE: PEG-PCL-PEG; RGCs: retinal ganglion cells

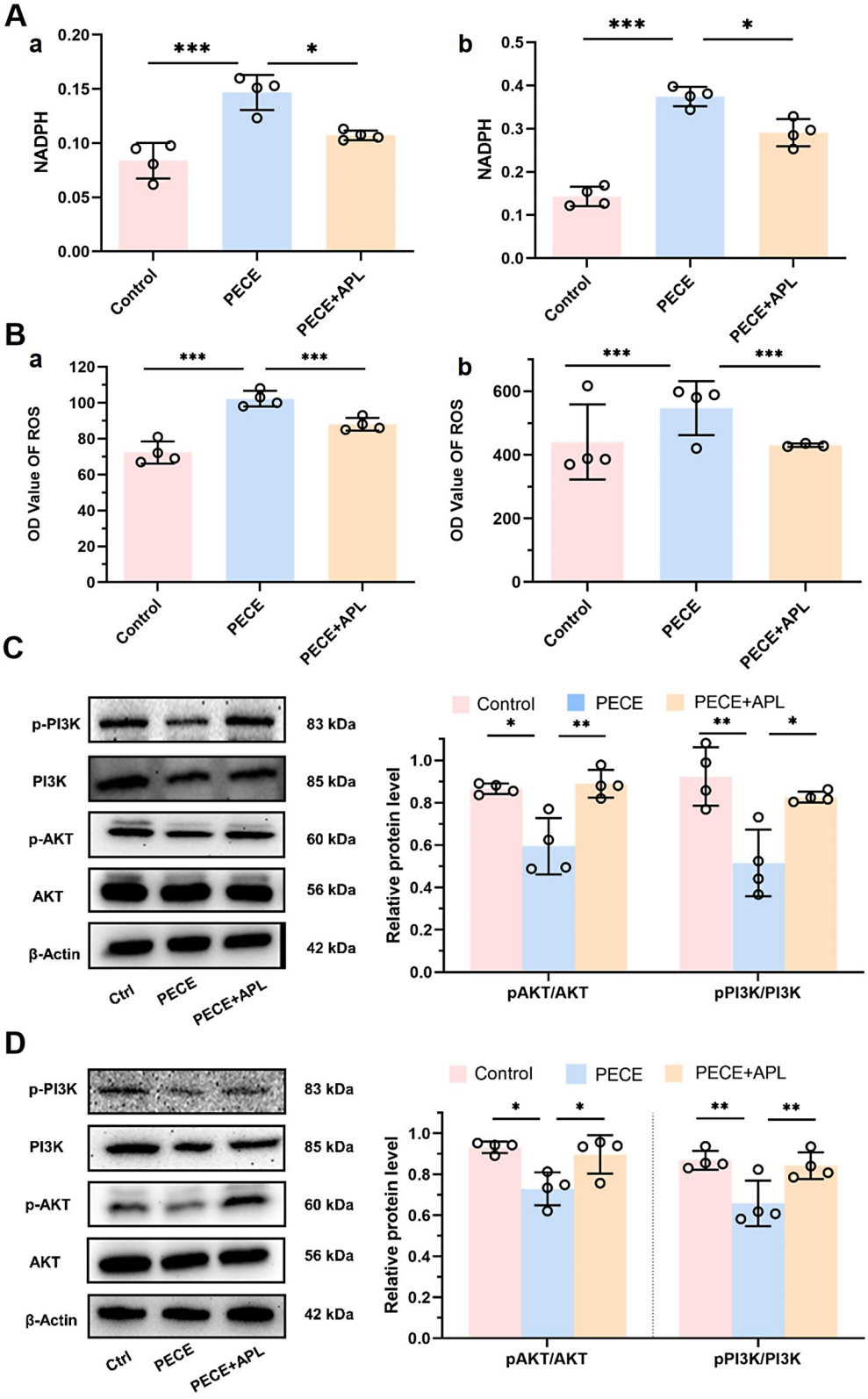

Fig. 5 (See legend on next page.)

(See figure on previous page.)

Fig. 5 Effects of exogenous apelin-13 on oxidative stress in retinal and brain neural tissue cells and the PI3K/Akt pathway. (**A**) a NADPH content was higher in retinal tissues in the PECE group than in the NC group, whereas it was lower in the Apelin-13 group than in the PECE group. (**A**) b NADPH levels in the brain tissues changed in the same pattern as those in the retina. (**B**) a ROS content in the retinal tissues was higher in the PECE group than in the NC group, but lower in the Apelin-13 group. (**B**) b Trend of ROS levels in the brain tissues was the same as that in the retinal tissues. (**C**) p-PI3K/PI3K and p-Akt/Akt ratios were lower in the retina in the PECE group, whereas they were restored in the Apelin-13 group. (**D**) Alterations in p-PI3K/PI3K and p-Akt/Akt ratios in the brain tissues were similar to those in the retina. *$P < 0.05$, **$P < 0.01$, ***$P < 0.001$. Akt: protein kinase B; NC: normal control; PECE: PEG-PCL-PEG; PI3K: phosphatidylinositol 3-kinase; ROS: reactive oxygen species

of glaucomatous RGCs [30]. A metabolomics study showed that reduced levels of pyruvate in the retina are associated with IOP, accompanied by disturbances in glucose metabolism before optic nerve degeneration occurs [31]. Hence, improving glucose metabolism in the visual conduction pathway may be a promising strategy for glaucoma treatment.

Apelin-13 has been observed for its role in glucose and lipid metabolism and the regulation of insulin secretion [32]. Recently, Apelin-13 was shown to improve pregnancy outcomes in mice with gestational diabetes, potentially by activating the PI3K/Akt pathway to improve glucose-lipid metabolism, thereby reducing damage caused by oxidative stress and inflammatory responses [18]. Moreover, a mouse model of glaucoma revealed a protective effect of Apelin-13 against optic nerve damage; however, the underlying mechanism remained unclear [21]. Our findings support the hypothesis that Apelin-13 protects against high-IOP-induced RGCs loss by activating the PI3K/Akt pathway to modulate the redistribution of energy metabolism in neurons.

Intriguingly, our results indicated that retinal microglia were markedly and abnormally activated after IOP elevation (Fig. 1D), whereas microglia in the visual cortex showed no significant changes (Fig. 2A), consistent with the findings reported by Lam et al. [33]. This lack of microglial activation in the visual cortex suggested that the loss of neuronal cells had not yet occurred in the visual cortex. Additionally, our results demonstrated that Apelin-13 modulates aberrant GLUT1 and GLUT3 expression and increases G6PD expression (Fig. 4D and E), suggesting its role in regulating metabolic redistribution and neuronal energy metabolism. Chronic neuronal degeneration is associated with dysregulation of glucose metabolism and oxidative stress. Neurons primarily metabolize glucose via the PPP to maintain their antioxidant status [34]. G6PD is a critical enzyme in the PPP and an antioxidant that protects neurons from oxidative stress. It produces NADPH, which neutralizes ROS produced by oxidative stress, thereby reducing oxidative stress [35]. Apelin-13 may induce a shift in the PPP. The activation of G6PD and PPP facilitates the cell-autonomous production of NADPH and maintains glutathione (GSH) levels in neurons to protect against acute and chronic oxidative stress, as well as attenuates stress-induced inflammatory responses and reactive gliosis [36]. This indicates the therapeutic value of G6PD activation in diseases, such as neuronal injury. Interestingly, our results showed contrasting trends of GLUT1 expression in brain tissues, as measured by immunofluorescence staining (Fig. 4A) and western blotting (Fig. 4E). This discrepancy may be attributed to the different distributions of GLUT1 and GLUT3. GLUT3 is primarily localized in neuronal membranes, whereas GLUT1 is mainly found in the BBB, glial cells, and microvascular endothelial cells [37]. The observed decrease in GLUT1 expression in the retinal and brain tissues may be related to the disruption of BBB integrity. GLUT1 plays a role in transporting glucose from the blood to the brain, whereas GLUT3 is primarily responsible for transporting glucose from the brain to neurons [38]. Notably, the ability of neurons to transport glucose is 12-fold greater than that of astrocytes, even at low interstitial glucose concentrations [39]. GLUT3 plays a central role in the brain, and its expression coordinates with glucose utilization in the brain in vivo [40]. Glucose deprivation can upregulate GLUT3 expression in neurons, as has been demonstrated both in vivo and in vitro. In hypoglycemic mice, GLUT3 mRNA expression is significantly higher in specific brain regions [41]. Nagamatsu et al. reported that both acute (1 day) and chronic (21 days) hypoxia induced glucose depletion and lactate release in rat primary cortical astrocytes, with the difference being that acute hypoxia increased GLUT1 expression, whereas chronic hypoxia decreased it [42]. Therefore, we speculated that 28 days after IOP elevation, long-term ischemia and hypoxia resulted in reduced GLUT1 expression and decreased glucose transport in the BBB and astrocytes, suggesting that GLUT1 and GLUT3 in neurons may have undergone a compensatory elevation to maintain the energy supply of neuronal cells. In addition, because of its key role in the brain, increased GLUT3 expression in neuronal cells may contribute to gradual compensatory increase in glucose uptake in the brain's visual cortex following a decrease in glucose uptake early in the course of elevated IOP, as shown on PET/MRI, in mice with high IOP in our study (Fig. 2B).

This study has several limitations that warrant further investigation. Firstly, our conclusions need to be further validated by additional research methods and larger sample sizes. Secondly, while GLUT1 and GLUT3 are reliable markers for assessing glucose transporter uptake, additional studies on intermediates of glucose metabolism are essential. Finally, further clinical studies are necessary to determine whether alterations in glucose uptake in the

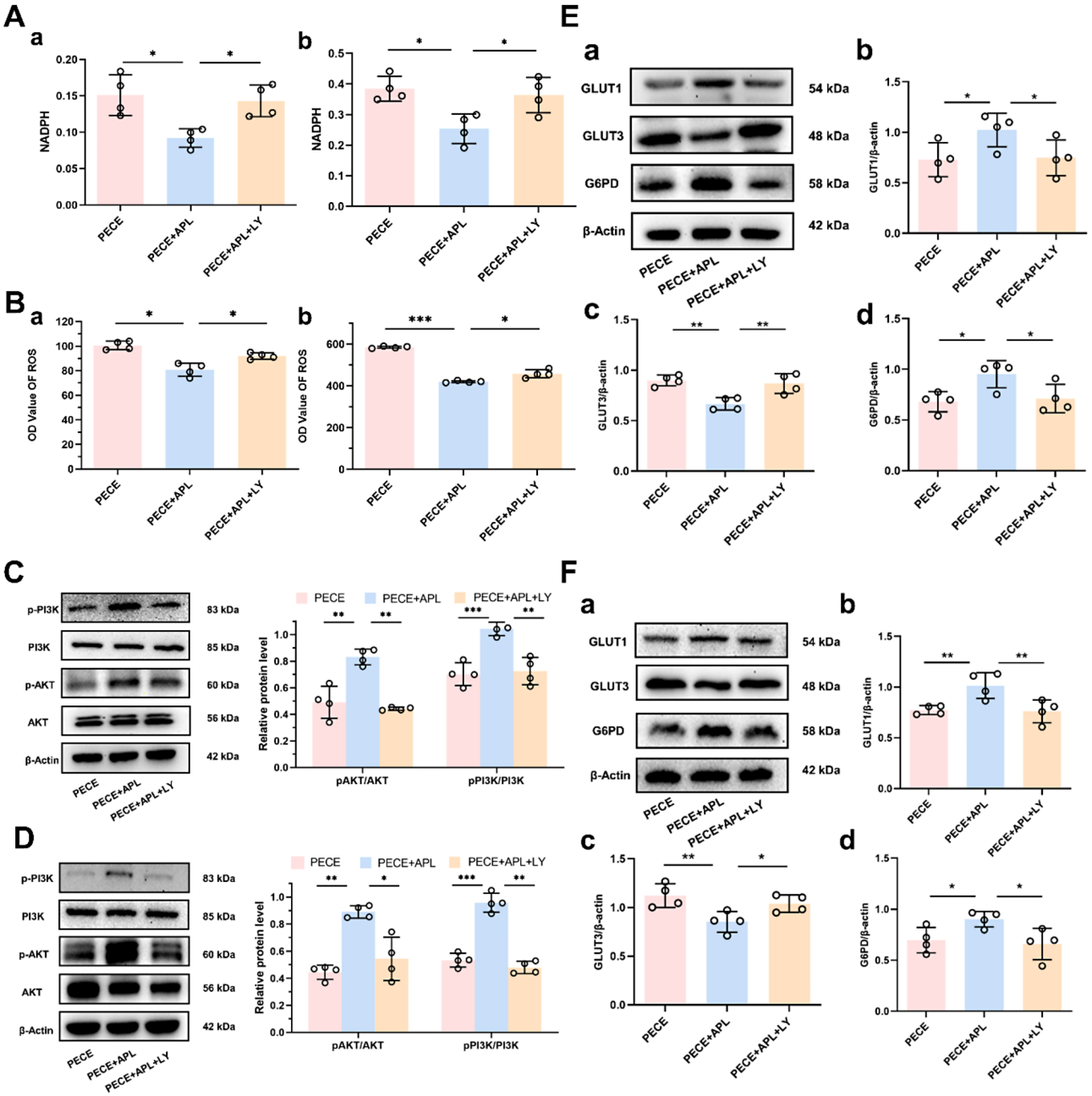

Fig. 6 Effects of Apelin-13 on oxidative stress and the protein regulation and the PI3K/Akt pathway in retinal and brain neural tissue cells can be reversed by LY294002. (**A**) a NADPH levels in the retinal tissue were lower in the Apelin-13 group than in the PECE group, whereas they were higher in the LY294002 group than in the Apelin-13 group. (**A**) b NADPH levels in the brain tissues changed in the same pattern as those in the retinal tissues. (**B**) a ROS levels in the retinal tissues were lower in the Apelin-13 group than in the PECE group and higher in the LY294002 group. (**B**) b Trend of ROS levels in the brain tissues was the same as that in the retinal tissues. (**C**) The p-PI3K/PI3K and p-Akt/Akt ratios in the retinal tissues of mice were significantly higher in the Apelin-13 group than in the PECE group, whereas these ratios were reduced in the LY294002 group. (**D**) Alterations in p-PI3K/PI3K and p-Akt/Akt ratios in the brain tissues followed the same trend as observed in the retinal tissues. (**E**) a GLUT1, GLUT3, and G6PD expression in the retina. (**E**) b GLUT1 expression reduced in the LY294002 group compared with the Apelin-13 group. (**E**) c GLUT3 expression was increased in the LY294002 group compared with the Apelin-13 group. (**E**) d G6PD expression was reduced in the LY294002 group compared with the Apelin-13 group. (**F**) a GLUT1, GLUT3, and G6PD expression in the brain. (**F** b, c, d Trend of GLUT1, GLUT3, and G6PD expression in the brain was consistent with that in the retinal tissues. *$P < 0.05$, **$P < 0.01$, ***$P < 0.001$. Akt: protein kinase B; IOP: intraocular pressure; PI3K: phosphatidylinositol 3-kinase; RGCs: retinal ganglion cells; ROS: reactive oxygen species

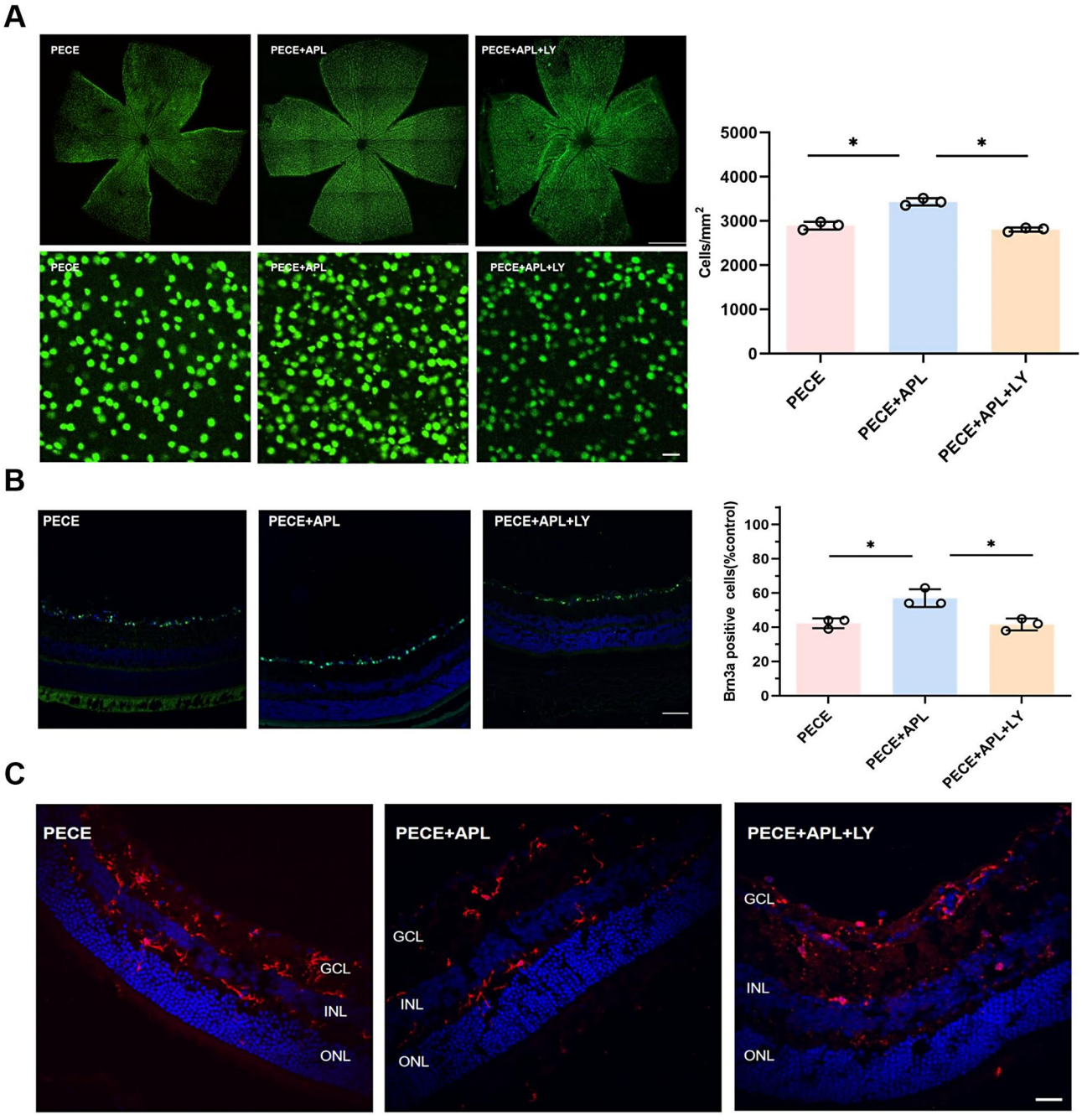

Fig. 7 Inhibition of the PI3K/Akt signaling pathway reduces the protective effect of Apelin-13 on optic nerve damage in mice with chronic high IOP. (**A**) The number of RGCs in the retina was reduced significantly in the LY294002 group compared with the Apelin-13 group. $n = 4$. (Green: Brn3a, scale bar: 500 μm in the upper panel and 50 μm in the lower panel). (**B**) Alterations in the number of RGCs were consistent with those in (**A**). $n = 4$. Green: Brn3a, scale bar: 50 μm. (**C**) A significantly greater number of microglia were activated and had migrated in the LY294002 group than in the Apelin-13 group. Red: Iba1, blue: DAPI, scale bar: 20 μm. $^{*}P < 0.05$, $^{**}P < 0.01$, $^{***}P < 0.001$. DAPI: 4′,6-diamidino-2-phenylindole; IOP: intraocular pressure; PECE: PEG-PCL-PEG; RGCs: retinal ganglion cells

visual center are related to the extent of glaucomatous disease.

In conclusion, alterations in glucose metabolism in the visual center may signify an early event in glaucomatous optic nerve damage. We surmise that Apelin-13 plays a neuroprotective role by regulating the redistribution of energy metabolism in RGCs and visual cortex neurons, thereby reducing the energy deficit induced by elevated IOP and activating the PPP to counteract oxidative stress. Although this study only focused on the 28 days after IOP elevation, and more permanent changes need to be

further investigated, it still provides some value for the study of the pathogenesis and prevention of glaucoma.

Supplementary Information

The online version contains supplementary material available at https://doi.org/10.1186/s12967-025-06212-z .

Supplementary Material 1

Acknowledgements
We sincerely thank the Sichuan Clinical Research Center for Neurosurgery of the Affiliated Hospital of Southwest Medical University for providing convenient experimental conditions and professional guidance on experimental techniques, and Professor Fu Shaozhi of the Department of Oncology of the Affiliated Hospital of Southwest Medical University for gifting the PECE hydrogel.

Author contributions
Ya Zhang partly designed the experiments and mainly completed the experiments, as well as wrote the manuscript. Jia Zhao assisted in completing the experiments and processed most of the data. Jian Zhou instructed the experimental methods and techniques. Zhen Jiang and Kaihui Cheng assisted in completing some of the experiments. Caifeng Lei completed some of the data processing, and Ling Yu designed the experiments, instructed the research direction, supported the project, and revised the manuscript. All authors read and approved the final manuscript.

Funding
This research is financed by the National Nature Science Foundation of China (grant No. 82070962).

Data availability
The data that support the findings of this study are available from the corresponding author upon reasonable request.

Declarations

Ethical approval
This study is approved by the Laboratory Animal Welfare Ethics Review Committee of the Third Military Medical University of the Chinese People's Liberation Army (grant No. AMUWEC2020033).

Competing interests
The authors declare no competing interests.

Author details
[1]Department of Ophthalmology, Daping Hospital, Army Medical Center, Army Medical University, Chongqing 400042, China
[2]Department of Ophthalmology, The Affiliated Hospital, Southwest Medical University, Luzhou, Sichuan 646000, China
[3]Department of Otolaryngology-Head and Neck Surgery, The Affiliated Hospital, Southwest Medical University, Luzhou, Sichuan 646000, China
[4]Department of Neurosurgery, The Affiliated Hospital, Southwest Medical University, Luzhou, Sichuan 646000, China

Received: 17 July 2024 / Accepted: 6 February 2025
Published online: 18 February 2025

References

1. Resnikoff S, Pascolini D, Mariotti SP, Pokharel GP. Global magnitude of visual impairment caused by uncorrected refractive errors in 2004. Bull World Health Organ. 2008;86:63–70.
2. Almasieh M, Levin LA. Neuroprotection in Glaucoma: animal models and clinical trials. Annu Rev Vis Sci. 2017;3:91–120.
3. Iezhitsa I, Agarwal R. New solutions for old challenges in glaucoma treatment: is taurine an option to consider? Neural Regen Res. 2021;16:967–71.
4. Yücel YH, Zhang Q, Weinreb RN, Kaufman PL, Gupta N. Effects of retinal ganglion cell loss on magno-, parvo-, koniocellular pathways in the lateral geniculate nucleus and visual cortex in glaucoma. Prog Retin Eye Res. 2003;22:465–81.
5. Gupta N, Ang LC, Noël de Tilly L, Bidaisee L, Yücel YH. Human glaucoma and neural degeneration in intracranial optic nerve, lateral geniculate nucleus, and visual cortex. Br J Ophthalmol. 2006;90:674–8.
6. Yücel Y, Gupta N. Glaucoma of the brain: a disease model for the study of transsynaptic neural degeneration. Prog Brain Res. 2008;173:465–78.
7. Coyle JT, Puttfarcken P. Oxidative stress, glutamate, and neurodegenerative disorders. Science. 1993;262:689–95.
8. Ames A 3rd, Li YY. Energy requirements of glutamatergic pathways in rabbit retina. J Neurosci. 1992;12:4234–42.
9. Yu DY, Cringle SJ, Balaratnasingam C, Morgan WH, Yu PK, Su EN. Retinal ganglion cells: energetics, compartmentation, axonal transport, cytoskeletons and vulnerability. Prog Retin Eye Res. 2013;36:217–46.
10. Duncan RO, Sample PA, Weinreb RN, Bowd C, Zangwill LM. Retinotopic organization of primary visual cortex in glaucoma: comparing fMRI measurements of cortical function with visual field loss. Prog Retin Eye Res. 2007;26:38–56.
11. Werner AC, Shen LQ. A review of OCT angiography in Glaucoma. Semin Ophthalmol. 2019;34:279–86.
12. Millecamps S, Julien J-P. Axonal transport deficits and neurodegenerative diseases. Nat Rev Neurosci. 2013;14:161–76.
13. Takihara Y, Inatani M, Eto K, Inoue T, Kreymerman A, Miyake S, et al. In vivo imaging of axonal transport of mitochondria in the diseased and aged mammalian CNS. Proc Natl Acad Sci U S A. 2015;112:10515–20.
14. Nita M, Grzybowski A. The Role of the Reactive Oxygen Species and Oxidative Stress in the Pathomechanism of the Age-Related Ocular Diseases and Other Pathologies of the Anterior and Posterior Eye Segments in Adults. Oxid Med Cell Longev. 2016, 1–23 (2016).
15. Wu X, Pang Y, Zhang Z, Li X, Wang C, Lei Y, et al. Mitochondria-targeted antioxidant peptide SS-31 mediates neuroprotection in a rat experimental glaucoma model. Acta Biochim Biophys Sin. 2019;51:411–21.
16. Schubert D. Glucose metabolism and Alzheimer's disease. Ageing Res Rev. 2005;4:240–57.
17. Patra KC, Hay N. The pentose phosphate pathway and cancer. Trends Biochem Sci. 2014;39:347–54.
18. Lee DK, Cheng R, Nguyen T, Fan T, Kariyawasam AP, Liu Y, et al. Characterization of apelin, the ligand for the APJ receptor. J Neurochem. 2000;74:34–41.
19. Cheng B, Chen J, Bai B, Xin Q. Neuroprotection of apelin and its signaling pathway. Peptides. 2012;37:171–3.
20. Coleman M, Kasai A, Kinjo T, Ishihara R, Sakai I, Ishimaru Y et al. Apelin Deficiency accelerates the progression of amyotrophic lateral sclerosis. PLoS ONE 6 (2011).
21. Ishimaru Y, Sumino A, Kajioka D, Shibagaki F, Yamamuro A, Yoshioka Y, et al. Apelin protects against NMDA-induced retinal neuronal death via an APJ receptor by activating Akt and ERK1/2, and suppressing TNF-α expression in mice. J Pharmacol Sci. 2017;133:34–41.
22. Zheng XD, Huang Y, Li H. Regulatory role of Apelin-13-mediated PI3K/AKT signaling pathway in the glucose and lipid metabolism of mouse with gestational diabetes mellitus. Immunobiology 226 (2021).
23. He C, Xiu W, Chen Q, Peng K, Zhu X, Wang Z et al. Gut-licensed $\beta7^{+}CD4^{+}$T cells contribute to progressive retinal ganglion cell damage in glaucoma. Sci Transl Med 15 (2023).
24. Yu L, Zheng Y, Liu BJ, Kang MH, Millar JC et al. Secreted protein acidic and rich in cysteine (SPARC) knockout mice have greater outflow facility. PLoS ONE 15 (2020).
25. Forrester J, Peters A. Nerve fibres in optic nerve of rat. Nature. 1967;214:245–7.
26. Cherry SR, Williams SP, Marik J, Walton JH, Judenhofer MS, Ouyang Y. Simultaneous PET/MRI imaging during mouse cerebral hypoxia-ischemia. J Vis Exp (2015).
27. Sato K, Saigusa D, Saito R, Fujioka A, Nakagawa Y, Nishiguchi KM et al. Metabolomic changes in the mouse retina after optic nerve injury. Sci Rep 8 (2018).
28. Murai H, Suzuki Y, Kiyosawa M, Tokumaru AM, Ishiwata K, Ishii K. Cerebral glucose metabolism in the striate cortex positively correlates with fractional anisotropy values of the optic radiation in patients with glaucoma. Clin Exp Ophthalmol. 2015;43:711–9.
29. Mergenthaler P, Lindauer U, Dienel GA, Meisel A. Sugar for the brain: the role of glucose in physiological and pathological brain function. Trends Neurosci. 2013;36:587–97.

30. Williams PA, Harder JM, John SWM. Glaucoma as a metabolic Optic Neuropathy: making the case for Nicotinamide treatment in Glaucoma. J Glaucoma. 2017;26:1161–8.
31. Harder JM, Guymer C, Wood JPM, Daskalaki E, Chidlow G, Zhang C, et al. Disturbed glucose and pyruvate metabolism in glaucoma with neuroprotection by pyruvate or rapamycin. Proc Natl Acad Sci U S A. 2020;117:33619–27.
32. Yue P, Jin H, Aillaud M, Deng AC, Azuma J, Asagami T, et al. Apelin is necessary for the maintenance of insulin sensitivity. Am J Physiol Endocrinol Metab. 2010;298:E59–67.
33. Lam D, Jim J, To E, Rasmussen C, Kaufman PL, Matsubara J. Astrocyte and microglial activation in the lateral geniculate nucleus and visual cortex of glaucomatous and optic nerve transected primates. Mol Vis. 2009;15:2217–29.
34. Spaans SK, Weusthuis RA, van der Oost J, Kengen SWM. NADPH-generating systems in bacteria and archaea. Front Microbiol 6 (2015).
35. Tu D, Gao Y, Yang R, Guan T, Hong J-S, Gao H-M. The pentose phosphate pathway regulates chronic neuroinflammation and dopaminergic neurodegeneration. J Neuroinflammation 16 (2019).
36. Tang BL. Neuroprotection by glucose-6-phosphate dehydrogenase and the pentose phosphate pathway. J Cell Biochem. 2019;120:14285–95.
37. Espinoza-Rojo M, Iturralde-Rodríguez KI, Chánez-Cárdenas ME, Ruiz-Tachiquín ME, Aguilera P. Glucose transporters regulation on ischemic brain: possible role as therapeutic target. Cent Nerv Syst Agents Med Chem. 2010;10:317–25.
38. Vannucci SJ, Maher F, Simpson IA. Glucose transporter proteins in brain: delivery of glucose to neurons and glia. Glia. 1997;21:2–21.
39. Simpson IA, Carruthers A, Vannucci SJ. Supply and demand in Cerebral Energy Metabolism: the role of nutrient transporters. J Cereb Blood Flow Metab. 2007;27:1766–91.
40. Simpson IA, Dwyer D, Malide D, Moley KH, Travis A, Vannucci SJ. The facilitative glucose transporter GLUT3: 20 years of distinction. Am J Physiol Endocrinol Metab. 2008;295:E242–53.
41. Nagamatsu S, Sawa H, Inoue N, Nakamichi Y, Takeshima H, Hoshino T. Gene expression of GLUT3 glucose transporter regulated by glucose in vivo in mouse brain and in vitro in neuronal cell cultures from rat embryos. Biochem J. 1994;300:125–31.
42. Véga C, Sachleben R, Gozal L, Gozal D. Differential metabolic adaptation to acute and long-term hypoxia in rat primary cortical astrocytes. J Neurochem. 2006;97:872–83.

Publisher's note